International Journal of Academic Multidisciplinary Research (IJAMR)
ISSN: 2643-9670
Vol. 7 Issue 11, November - 2023, Pages: 251-260

Dynamic Modelling and Simulation of Single-Cage Induction Machine for Transient Response Performance Analysis

I. M. Uneze1, I. U. Uju2, C. O. Uneze3

1Department of Electrical and Electronics Engineering, Imo State Polytechnic, Omuma, Nigeria
unezeijeoma@gmail.com
2Department of Electrical and Electronics Engineering, Chukwuemeka Odumegwu Ojukwu University, Uli, Nigeria
ujuisidore@yahoo.co.uk
3Department of Software Engineering, Federal University of Technology Owerri, Owerri, Nigeria
odochi1982@gmail.com

***Abstract**: The simulation analysis of the transient response performance of a single cage machine has been conducted in MATLAB/Simulink environment. Having obtained the mathematical model of an induction motor based on Park's transformation in d-q reference frame, a Simulink model was developed to investigate the behaviour of the motor under no load, half load and full load conditions. The Simulation results have shown that increasing load torque affects the transient and steady state efficiency of induction machine. Generally, the transient behaviour of the single cage motor under no load is that its rise time (or response time) to input signal was 0.81 s, settling time (time to settle or reached steady state) was 1.09 s, and the steady-state speed was 1500 rpm. At half loading, its rise time was 1.23 s, settling time was 1.58 s, and it steady-state speed was 1463 rpm. At full load, the rise time in this case was 2.18 s, the settling time was 2.98 s, and the speed at steady-state was 1415 rpm.*

Keywords—Induction machine; MATLAB/Simulink; Single-cage; Transient response

1. INTRODUCTION

All sorts of electro-mechanical drive systems largely employ induction machines due to their simple and robust structure. Induction machines have become favourable alternative to direct current (DC) machines for variable speed applications because of the recent development in control techniques that involves used of power electronics and microprocessors. Thus, in applications that require speed variation, alternating current (AC) machines are considered good replacement for DC machines.

Generally, all rotating electrical machine can be divided into a stationary part, the stator, and a rotating part, the rotor. In between the rotor and stator is a small air gap which is assumed to be narrow and uniform. The stationary part of the machine has three identical stator windings mechanically placed at an angle of 120^0. These stator windings are considered to be sinusoidally distributed along the stator circumference. In case of a wound-rotor the rotor construction is similar to that of the stator. Squirrel cage rotors however are made up of two end rings and a number of rotor bars. This cage acts as a set of short-circuited windings. The symmetrical squirrel cage can therefore be seen as a small number of lumped windings assuming that the rotor material is same. If magnetic saturation is neglected, the rotor "windings" may be represented as three identical, short-circuited, lumped windings, like the stator windings, positioned at an angle of 120^o mechanical degrees (Veltman, 2006).

In normal operation the rotor rotates slower than the applied stator field, which causes an induced voltage in the shorted windings. This voltage will generate a current flow through the rotor windings (bars). The magnetic field produced by the stator penetrates the rotor winding and, therefore, torque will be generated. If the rotor speed equals the rotation speed of the stator field (synchronous speed), no voltage is induced and consequently no torque is generated. The relative difference between the stator field rotation speed and the mechanical rotor speed is defined as slip.

In this paper simulation of three-phase induction machine is carried out to evaluate its transient response performance characteristics considering the rise time and settling time for no loading, half loading and full loading in terms of current, torque and speed.

2. LITERATURE REVIEW

The part of a three-phase induction motor that is stationary is the stator and corresponds to the York of a DC motor. Depending on the required rotor speed, the stator is wound to provide a 6-pole, 4-pole, or 2-pole rating magnetic field, equivalent to DC motor armature; it is constructed with laminated iron so as to reduce eddy currents. For induction motor of the squirrel cage type, aluminum or copper bars placed in slots cut in the laminated ring. Figure 1shows an axial sectional view of squirrel cage induction motor.

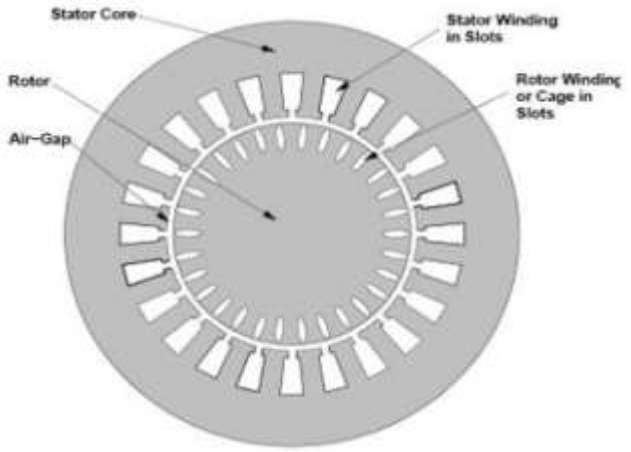

Fig.1 *Axial section of squirrel cage induction motor*

As shown in Fig.1, the arrangement comprises a laminated stator core with stator winding in slots. Also, the rotor consists of rotor winding or cage in slots. In order to achieve better starting and improved running, the slots are skewed. There are no external connections for this type of rotor, which means slip ring and brushes are not required. Squirrel-cage motor is considered a cheap, efficient and reliable induction machine.

The application of three-phase supply to the stator windings causes a rotating magnetic field. Consequently, a magnetic flux is produced that cuts on a rotor bar resulting in induced electromotive force (e.m.f) or voltage in it. Given that the bar is connected through the end conducting rings to another bar on pole pitch away, current flows in the bars. The interaction of the associated magnetic field due to the current carrying conductors (bars) and the rotating magnetic field produces a force that that tends to the rotor in the same direction as the rotating magnetic field. All the rotor conductors experience similar forces such that a torque is generated causing the rotor to rotate.

Several studies regarding simulation and modelling of three-phase induction machine have been carried out. For instance, hybrid simulated annealing-evaporation rate water cycle algorithm (SA-ERWCA) was applied to estimate the equivalent circuit parameter of induction machine by Ćalasan et al. (2020). Fuzzy logic approach was used for simulating an induction machine (Chitra and Prabhakar, 2006). Motor parameters were predicted using genetic algorithms (GA) by Elnaghi et al. (2019). Due to limited information shared by the manufacturer's datasheets, Gübahçe et al. (2022) carried out equivalent circuit parameters of induction motor. Artificial neural network (ANN) and an adaptive neuro-fuzzy system (ANFIS) were utilized by Jirdehi and Rezaei (2016)to simulate induction motor. The performance of dual-rotor permanent magnet induction motor (DRPMIM) was improved by Diao (2015) using Maxwell Ansolf software. Park's transformation was employed by Salkumar et al. (2020) to develop the mathematical models of three-phase and five-phase induction motors. Ogunjuyigbe et al. (2018) studied the transient and dynamic performance evaluation of a dual stator-winding induction machine with squirrel cage rotor. A two-dimensional transient numerical evaluation of three-phase induction motor with a deep bar squirrel cage rotor under a voltage-forced operation was performed by Hong and Hwang (2012). Simulations of induction motor in static and dynamic conditions were carried out by Le Roux and Ngwenyama (2022).

3. MATHEMATICAL MODELLING OF SQUIREL-CAGE MACHINE

The equations that describe the dynamic characteristics of squirrel-cage operation are presented in this section. Analyzing performance of induction motor, requires the developing a mathematical model. Electrical machine dynamics are usually represented in either state space form or as a transfer function. Consequently, the equivalent circuits of induction motor in direct axis and quadrature axis (d-q axis) as shown in Fig. 2 and 3 is employed in the dynamic description of induction motor.

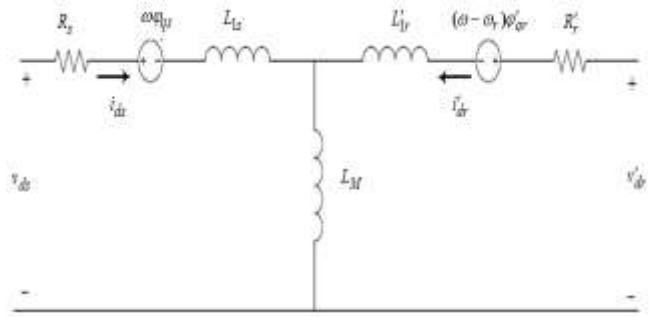

Fig. 2 *Equivalent circuit of induction machine in d-reference axis*

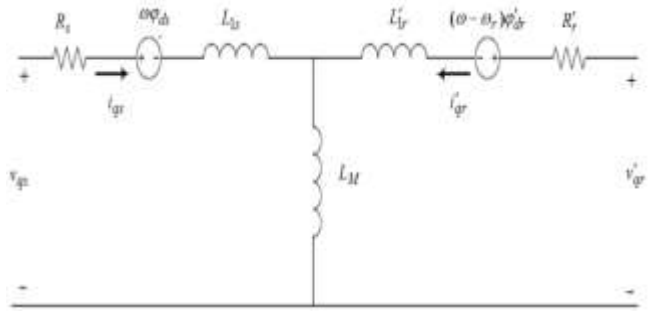

Fig. 3 *Equivalent circuit of induction machine in q-reference axis*

The voltage required to drive the flux and torque to the expected values within a given time period is calculated using induction motor model (Idoko et al., 2017). The dynamic model of the induction motor in Simulink is used to analyze the calculated voltage.

It is essential to make the assumption that the rotor bars are short circuited and there is no load, when deriving the mathematical equations representing the dynamic behaviour of

the induction motor (Malatji, 2020). It should be noted that all variables shown in Fig. 2 and 3 all through this mathematical formulation are referred to the stator.

The Park Transformation of the 3-phase stationary reference variables a-b-c that are 120^o apart in 2-phase stationary reference axis d-q is used to start the modeling of induction machine. Assuming that d-q axes are tilting at an angle of θ, the direct axis voltage v_d and quadrature axis voltage v_q can be resolved into a-b-c component and then written in vector-matrix form as:

$$\begin{bmatrix} v_q \\ v_d \\ v_0 \end{bmatrix} = \frac{2}{3}\begin{bmatrix} \cos\theta & \cos(\theta-\gamma) & \cos(\theta-\gamma) \\ \sin\theta & \sin(\theta-\varphi) & \sin(\theta+\varphi) \\ 0.5 & 0.5 & 0.5 \end{bmatrix} v_{abc} \quad (1)$$

where v_0 is added as zero sequence element that may or may not be present. Also, v_a, v_b, v_c are the various voltages resolved into a-b-c component. Equation (1) can be simplified further as shown in Equation (2) and (3):

$$v_{dq0} = [K_s][v_{abc}]$$

$$(2)\ v_{dq0} = \begin{bmatrix} v_q \\ v_d \\ v_0 \end{bmatrix},\ K_s = \frac{2}{3}\begin{bmatrix} \cos\theta & \cos(\theta-\gamma) & \cos(\theta-\gamma) \\ \sin\theta & \sin(\theta-\varphi) & \sin(\theta+\varphi) \\ 0.5 & 0.5 & 0.5 \end{bmatrix},$$

$$v_{abc} = \begin{bmatrix} v_a \\ v_b \\ v_c \end{bmatrix} \quad (3)$$

The d-q reference axis derivation is further presented in mathematical form, which is followed by a circuit analysis technique. The concept by Leedy (2013) is considered in this work as follows using Fig. 2 and 3.

$$v_{dq0s} = R_s i_{dq0s} + \omega\varphi_{dq0s} + d\varphi_{dq0s}/dt \quad (4)$$

$$v_{dq0r}\varphi'_{dq0r} = R_r i'_{dq0r} + (\omega-\omega_r)\varphi'_{dq0r} + d\varphi'_{dq0r}/dt \quad (5)$$

where v_{dq0s} is the d-q axis stator voltage, R_s is the stator resistance, i_{qd0s} is the d-q axis stator current, ω is the electrical speed, $_{dq0s}$ is the d-q axis flux linkage in the stator variable, v_{dq0r} is the d-q axis rotor voltage, φ'_{dq0r} is the is d-q axis flux linkage in the rotor variable, R_r is the rotor resistance, i'_{dq0r} is the d-q axis rotor current, ω_r is the rotor electrical speed.

The d-q flux linkages in the stator and rotor variables are defined as given by:

$$\begin{bmatrix} \varphi_{dq0s} \\ \varphi'_{dq0s} \end{bmatrix} = \begin{bmatrix} K_s L_s K_s^{-1} & K_s L_{sr} K_r^{-1} \\ K_r (L'_{sr})_T K_s^{-1} & K_r L'_r K_r^{-1} \end{bmatrix} \begin{bmatrix} i_{da0s} \\ i'_{dq0r} \end{bmatrix} \quad (6)$$

$$K_s L_s K_s{}^1 = \begin{bmatrix} L_{Is}+L_M & 0 & 0 \\ 0 & L_{Is}+L_M & 0 \\ 0 & 0 & L_{Is}+L_M \end{bmatrix}, \quad (7)$$

$$L_M = \frac{3}{2}L_m$$

Similarly,

$$K_r L_r K_r^{-1} = \begin{bmatrix} L_{Isr}+L_M & 0 & 0 \\ 0 & L_{Ir}+L_M & 0 \\ 0 & 0 & L_{Ir}+L_M \end{bmatrix} \quad (8)$$

and

$$K_s L_{sr} K_r^{-1} = K_r (L'_{sr})_T K_s^{-1} = \begin{bmatrix} L_M & 0 & 0 \\ 0 & L_M & 0 \\ 0 & 0 & L_M \end{bmatrix} \quad (9)$$

Thus, the derivation of d-q flux formulae is determined from the following matrix:

$$\begin{bmatrix} \varphi_{qs} \\ \varphi'_{qr} \\ \varphi_{ds} \\ \varphi'_{dr} \end{bmatrix} = \begin{bmatrix} L_{ss} & L_M & 0 & 0 \\ L_M & L_{rr} & 0 & 0 \\ 0 & 0 & L_{ss} & L_M \\ 0 & 0 & L_M & L_{rr} \end{bmatrix} \begin{bmatrix} i_{qs} \\ i'_{qr} \\ i_{ds} \\ i'_{dr} \end{bmatrix} \quad (10)$$

where $K_s L_s K_s{}^1$, $K_r L_r K_r{}^1$, and $K_s L_{sr} K_r{}^1$ are the stator mutual inductance, rotor mutual inductance, and stator-rotor mutual inductance, L_{Is} is the stator inductance, L_{Ir} is the rotor inductance, L_m is the mutual winding inductance, $_{ds}$, $_{qs}$, $'_{dr}$ and $'_{qr}$ are the flux linkages for the stator d-axis/q-axis and the rotor d-axis/q-axis, i_{ds}, i_{qs}, i'_{dr} and i'_{qr} are the stator current for d-axis/q-axis and the rotor current for d-axis/q-axis respectively.

Now, further application is made using the equivalent circuit diagram in Fig. 2 and 3 to carry out circuit analysis from the d-axis and q-axis circuits to determine the d-axis and q-axis stator and rotor voltages. Hence, the d-axis and q-axis voltages of the stator are given by:

$$v_{qs} = R_s i_{qs} + \omega\varphi_{ds} + d\varphi_{qs}/dt \quad (11)$$

$$v_{ds} = R_s i_{ds} - \omega\varphi_{qs} + d\varphi_{ds}/dt \quad (12)$$

$$v'_{qr} = R'_r i'_{qr} + (\omega - \omega_r)\varphi'_{dr} + d\varphi'_{qr}/dt$$
(13)

$$v'_{dr} = R'_r i'_{dr} - (\omega - \omega_r)\varphi_{qr} + d\varphi_{dr}/dt$$
(14)

The flux linkages given in Eq. (10) are further defined by the following equations:

$$\varphi_{qs} = L_{Is} i_{qs} + L_m\left(i_{qs} + i'_{qr}\right)$$
(15)

$$\varphi_{ds} = L_{Is} i_{ds} + L_m\left(i_{ds} + i'_{dr}\right)$$
(16)

$$\varphi'_{qr} = L'_{Ir} i'_{qr} + L_m\left(i_{qs} + i'_{dr}\right)$$
(17)

$$\varphi'_{dr} = L'_{Ir} i'_{dr} + L_m\left(i_{qs} + i'_{dr}\right)$$
(18)

It is important to transform the reluctance of the stator, the rotor, and the mutual winding to inductance so as to calculate the current and flux linkages. In order to achieve this transformation, the relationship between reluctance and inductance for alternating current circuit is employed as follows:

$$L_{Is} = \frac{X_s}{2\pi f}$$
(19)

$$L_{Ir} = \frac{X_r}{2\pi f}$$
(20)

In the same vein, the inductance of the mutual winding is given by:

$$L_m = \frac{\frac{2}{3}X_s}{2\pi f} \text{ or } L_M = \frac{X_s}{2\pi f} \quad (21)$$

Thus, the self-inductance of the stator and rotor are given by:

$$L_s = L_m + L_{Is} \quad (22)$$

$$L_r = L_m + L_{Ir} \quad (23)$$

where X_S and X_r are stator and rotor reluctance. Solving for d-axis/q-axis stator and rotor current as shown in Fig. 2 and 3 in terms of flux linkages results in (Malatji, 2020):

$$i_{ds} = {}_{ds}\frac{L_r}{L_s L_r \quad L_m^2} \quad {}'_{dr}\frac{L_r}{L_s L_r \quad L_m^2}$$
(24)

$$i_{qs} = {}_{qs}\frac{L_r}{L_s L_r \quad L_m^2} \quad {}'_{qr}\frac{L_r}{L_s L_r \quad L_m^2}$$
(25)

$$i'_{dr} = \varphi'_{dr}\frac{L_r}{L_s L_r - L_m^2} - \varphi_{ds}\frac{L_r}{L_s L_r - L_m^2}$$
(26)

$$i'_{qr} = \varphi'_{qr}\frac{L_r}{L_s L_r - L_m^2} - \varphi_{qs}\frac{L_r}{L_s L_r - L_m^2}$$
(27)

Rate of flux linkages of the stator and rotor in terms of d-axis and q-axis variable elements can be computed as follows:

$$\frac{d\varphi_{ds}}{dt} = v_{ds} - \varphi_{ds}\frac{R_s L_r}{L_r L_s - L_m^2} + \varphi'_{dr}\frac{R_s L_m}{L_r L_s - L_m^2} + \omega\varphi_{qs}$$
(28)

$$\frac{d\varphi_{qs}}{dt} = v_{qs} - \varphi_{ds}\frac{R_s L_r}{L_r L_s - L_m^2} + \varphi'_{qr}\frac{R_s L_m}{L_r L_s - L_m^2} + \omega\varphi_{ds} \quad (29)$$

$$\frac{d\varphi'_{dr}}{dt} = 0 - \varphi'_{dr}\frac{R_r L_s}{L_r L_s - L_m^2} + \varphi_{ds}\frac{R_r L_m}{L_r L_s - L_m^2} + (\omega - \omega_r)\varphi'_{qr}$$
…… (30)

$$\frac{d\varphi'_{qr}}{dt} = 0 - \varphi'_{qr}\frac{R_r L_s}{L_r L_s - L_m^2} + \varphi_{qs}\frac{R_r L_m}{L_r L_s - L_m^2} + (\omega - \omega_r)\varphi'_{dr}$$
……. (31)

The d-q modeling of squirrel-cage machine is completed by Equation (31). The implementation of d-q model induction motor will be carried out in MATLAB/Simulink environment. The electrical torque (T_e) of induction motor and rotor speed can be computed using the following equations (Malatji, 2020):

$$T_e = \frac{3pL_m}{4}\left(i_{qs} i'_{dr} - i_{ds} i'_{qr}\right)$$
(32)

$$\frac{d\omega_r}{dt} = \frac{T_e \quad B\omega_r}{J}$$
(33)

where B, J are the friction coefficient and rotor initial respectively.

The implementation to examine d-q model squirrel-cage machine will be performed in MATLAB/Simulink environment as shown in Fig. 4.

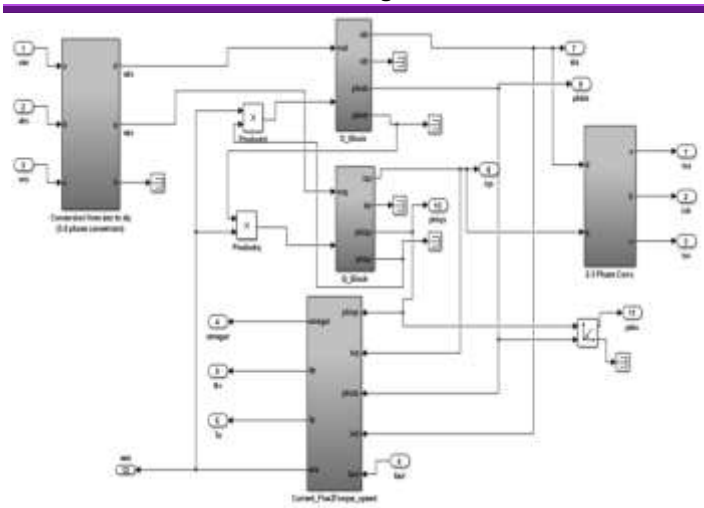

Fig. 4 *Simulink model of induction motor in d-q reference frame*

Table 1: Simulation parameters

Motor Parameter Definition	Symbol	Value
Stator resistance	R_s	3.5 Ω
Stator reactance	X_s	2.17 Ω
Single cage rotor resistance	R_r	3.16 Ω
Single cage rotor reactance	X_r	2.14 Ω
Line to line voltage	V_n	400 V
Rotor speed	ω_m	1500 rpm
Moment of inertia	J	0.102 $Jkg.m^2$
Friction coefficient	F	0 N.m.s
Number of poles	*p*	2
Nominal power	P	37.3 kW

4. RESULTS AND DISCUSSION

In this section, the result of the simulations conducted using MATLAB/Simulink models of three-phase squirrel cage motor are presented assuming constant and varying mechanical input (load) torque. The machine is fed from a 400 V, 50 Hz supply. The performance analysis of the induction machine has been presented in terms of single cage and double cage regarding the transient characteristics of the stator current (or line current), rotor current, torque, speed, and torque versus speed during starting given that the machine is not loaded (that is operating at no load), the machine is 50% loaded (operating at 50% loading), and the machine is 100% loaded (operating at full load) in steady state or constant load case.

4.1 Simulation with Machine Unloaded

This subsection presents the simulation results for single cage machine under no load in terms of line (stator) currents (Fig. 5a), rotor current (Fig. 5b), load torque (Fig. 6a), torque versus speed (Fig. 6b), and speed (Fig. 7) under no load.

Figure 5a Line (stator) currents under no load. The stator current waveforms for a, b, c reference frame are shown in Figure 4.2a considering the single cage configuration. It can be seen that the magnitude of the current was very high (20.2 A) at the start of the machine but reduces to 3.297Aafter 1.09 s and maintained this value as the machine reaches it rated speed at no load.

Figure 5b is the rotor current waveforms in terms of a, b, c reference frame under no load conditions for single cage mode. It can be seen that just like the stator current, the magnitude of the current was high (20.2 A) during the starting of the machine but reduces to 1.311e-07 A after 1.09 s when the motor reached steady operating speed.

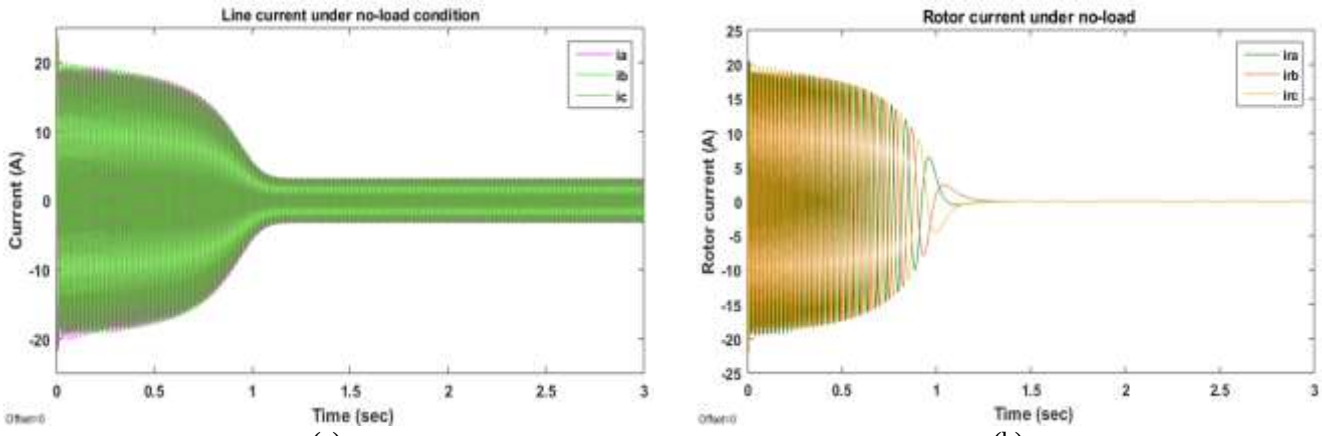

(a) (b)

Fig. 5: (a) Line (stator) currents and (b) Rotor currents under no load

International Journal of Academic Multidisciplinary Research (IJAMR)
ISSN: 2643-9670
Vol. 7 Issue 11, November - 2023, Pages: 251-260

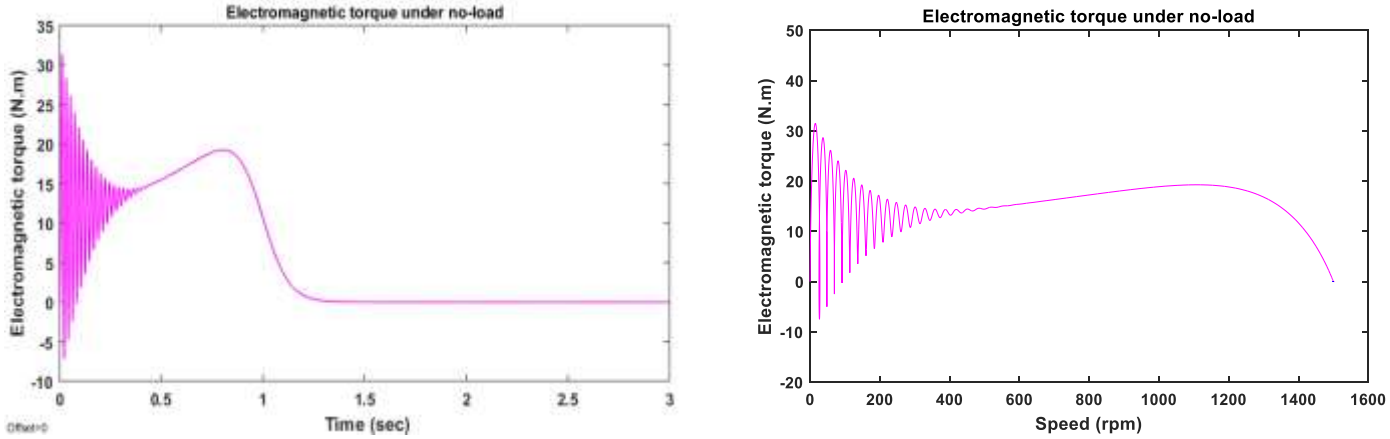

(a) (b)

Fig. 6 *(a) Torque and (b) Torque against speed under no load*

The single cage motor torque plot against time is shown in Fig. 6a for no load condition. The torque curve reveals that the motor has a starting of 31.38 Nm but after 1.09 s, a torque of near zero was reached as it began to run at the rated speed.

Figure 6b is the curve of electromagnetic torque against rotor speed for single cage mode simulated in 3 s. The simulation curve indicates that the torque was high during the starting of the motor but decreases as the motor reaches it rated speed.

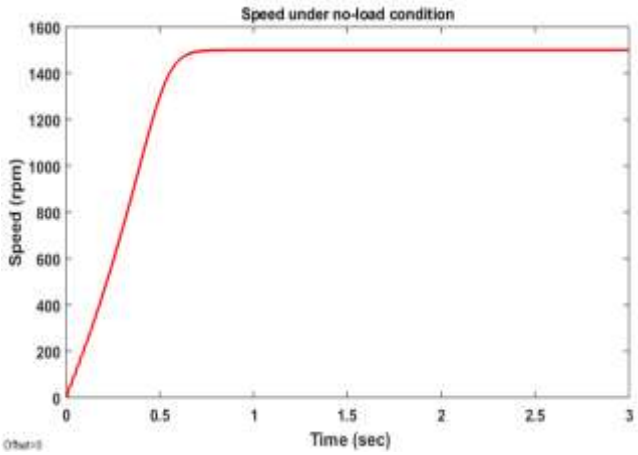

Fig. 7 *Motor Speed under no load*

Figure 7 is the curve of the rotor speed against time for single cage mode at no load. The curve reveals that the motor speed increases steadily from zero and reaches a steady-state value of 1500 rpm after 1.09 s, which is the rated speed of the motor.

In Fig. 5a and 5b, the three-phase current waveforms of the stator (line current) and the rotor are presented. As can be seen in Fig. 5a, the starting current in the transient state is very high, which is one of the characteristics of an induction machine. Regarding Fig. 6a, it is seen that during the transient state, the electromagnetic torque (Te) oscillates and then stops and subsequently moves towards the load torque. Similarly, the same oscillation characteristic in the transient state is observed in Fig. 6b with the electromagnetic torque plotted against machine speed. Also, in Fig. 7, a small disturbance is seen at the start of the speed. This is because of the oscillation in the starting electromagnetic torque of the machine. Nevertheless, as a result of no load, the machine attains a maximum point that is equal to the synchronous speed (1500 rpm) and maintains a steady-state while the torque goes to zero (because of no load torque or 0 Nm load torque) with decreased line current and rotor current. Generally, the transient behaviour of the single cage motor at this time is that its rise time (time to significantly respond) to input signal was 0.81 s, settling time (time to settle or reached steady state) was 1.09 s.

4.2 Simulation of Machine Under 50% Loading

The steady-state transient characteristics of the machine with single cage rotor configuration under 50% loading are presented in this subsection. The simulation in this case has assumed 50% loading taking the load torque to be 5 Nm. The performance is presented for line current in Fig. 8a, rotor current in Fig. 8b, electromagnetic torque in Fig. 9a, electromagnetic torque against speed in Fig. 9b, and speed in Fig. 10.

Figure 8a is the stator current waveforms for a, b, c reference frame considering the single cage configuration when the motor is running under 50% loading. It can be seen that the magnitude of the current was very high (20.2 A) at the start of the machine but reduces to 3.78 A after 1.58 s and maintained this value as the machine reaches its steady speed at half load.

Figure 8b is the rotor current waveforms in terms of a, b, c reference frame under 50%loading for single cage mode. It can be seen that just like the stator current, the magnitude of the current was high (20.2 A) during the starting of the machine but reduces to 2.035A after 1.58 s when the motor reached steady operating speed.

International Journal of Academic Multidisciplinary Research (IJAMR)
ISSN: 2643-9670
Vol. 7 Issue 11, November - 2023, Pages: 251-260

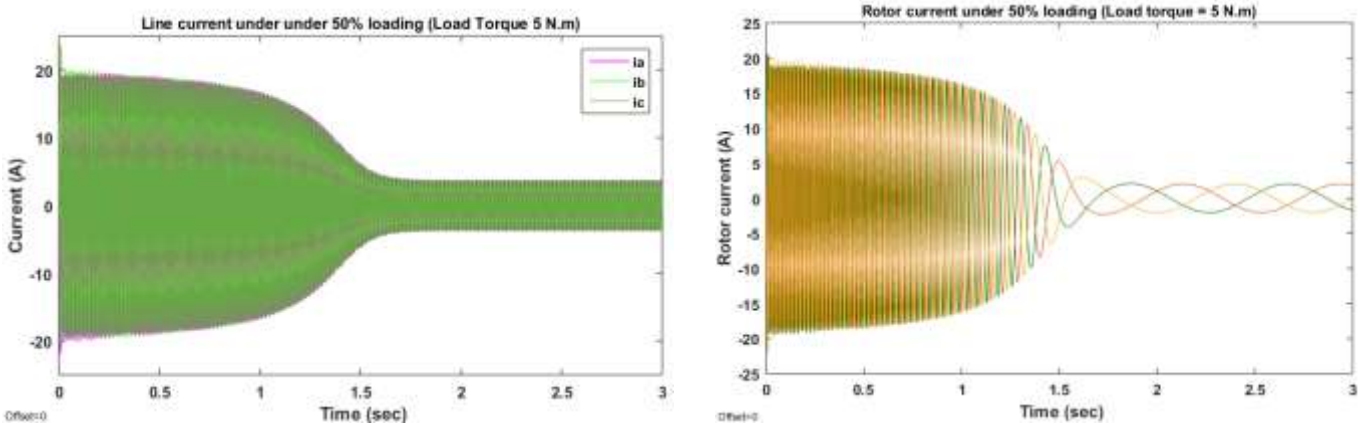

(a) (b)

Fig. 8 *(a) Line currents and (b) Rotor currents under 50% loading*

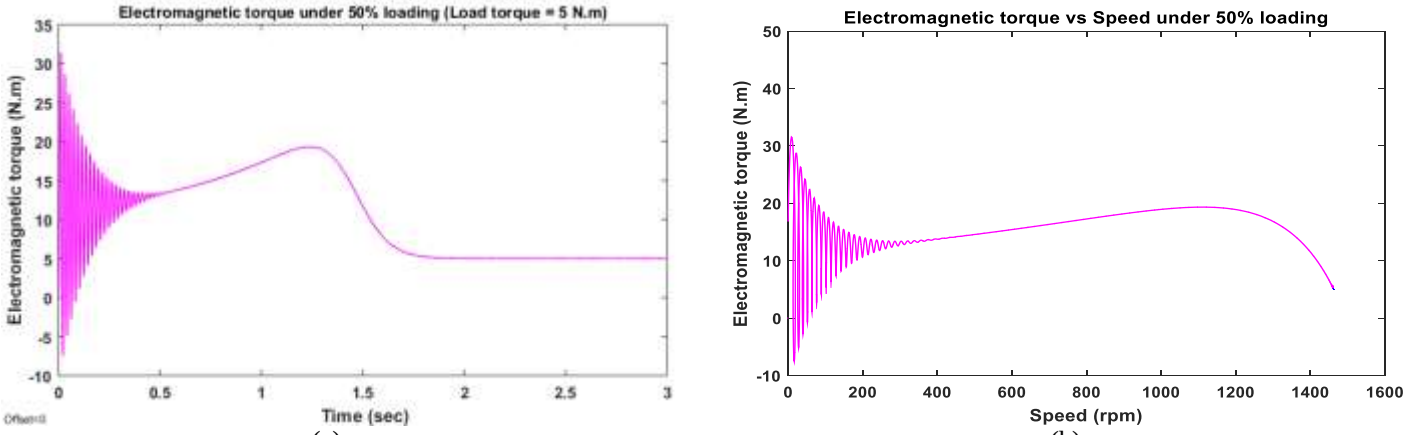

(a) (b)

Fig. 9 *(a) Torque and (b) Torque against speed under 50% loading*

The single cage motor torque plot against time is shown in Fig. 9a under 50% loading condition. The torque curve shows that the motor has a starting of 31.38 Nm but after 1.58 s, a torque of 5 Nm corresponding to the load torque was reached as it began to run at a steady speed.

Figure 9b is the curve of electromagnetic torque against rotor speed for single cage mode simulated in 3 s when the machine is running under 50% loading. The simulation curve indicates that the torque was high during the starting of the motor but decreases as the motor reaches its steady speed less than the rated speed due to loading effect.

Figure 10 shows the single cage rotor speed transient characteristic of during 50% loading. The speed response curve indicates that due to 50% loading, the speed of the dropped from the rated value (1500 rpm) to 1463 rpm. Thus, the effect of the half loading on the speed of the motor is 2.5% drop in rated speed.

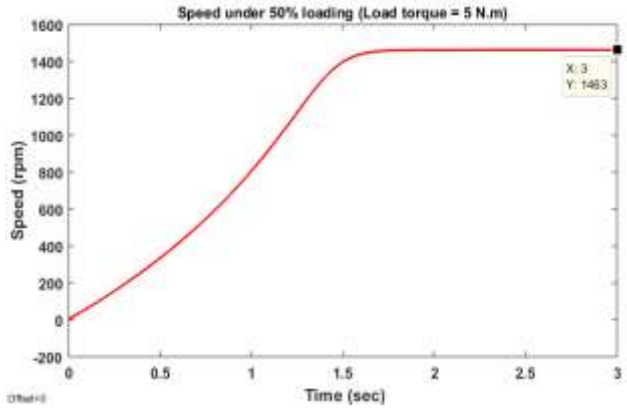

Fig. 10 *Motor Speed under 50% loading*

As shown in Fig. 8a and Fig. 9a, it can be seen that the machine reached the steady-state nearly 0.5 second later compared to no load condition. That is, with connected load torque, the machine takes longer time to reach steady state. This is expected as a result of increase in load torque. Looking at Fig. 8a-b, the amplitude (or magnitude) of the line current

and the rotor current were not affected by the increased magnitude of the load (torque). Hence, it suffices to say that the machine current is not affect by the external load and it is only a function of the parameters of the machine. As shown in Fig. 9b, the torque terminates at 5 Nm and at a speed less than the synchronous speed. In Fig. 10, the maximum speed attained is lower than with no load. Generally, the transient behaviour of the single cage motor under this condition is that its rise time to input signal was 1.23 s and settling time was 1.58 s.

4.3 Simulation of Machine under 100% Loading

The single cage rotor configuration under 100% loading is presented in this subsection. The steady-state transient characteristics of the machine are examined via simulation in this assuming a load of torque 10 Nm loading is connected to the machine. The behaviour of the machine is presented in terms of line current in Fig. 11a, rotor current in Fig. 11b, electromagnetic torque in Fig. 12a, electromagnetic torque against speed in Fig. 12b, and speed in Fig. 13.

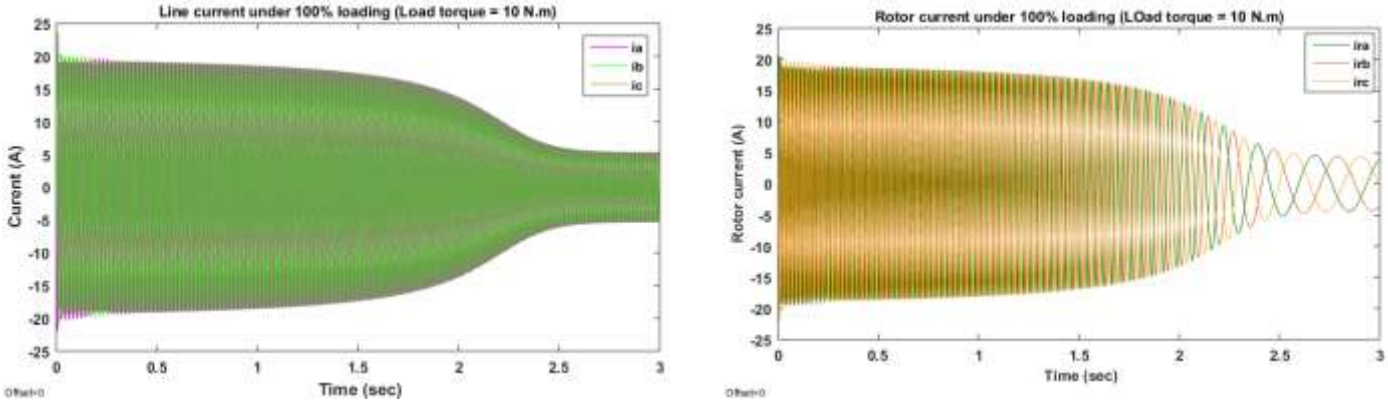

(a) (b)

Fig. 11 *(a) Line currents and (b) Rotor currents under 100% loading*

In Fig. 11a, the stator current waveforms for a, b, c reference frame considering the single cage configuration when the motor is running under 100% loading, shows that the magnitude of the current was very high (20.2 A) at the start of the machine but reduces to 5.35 A after 2.98 s and maintained this value as the machine reaches its steady speed at full load.

Figure 11b is the rotor current waveforms in terms of a, b, c reference frame under 100% loading for single cage mode. The magnitude of the current was high (20.2 A) during the starting of the machine but reduces to 4.35 A after 2.98 s when the motor reached steady operating speed.

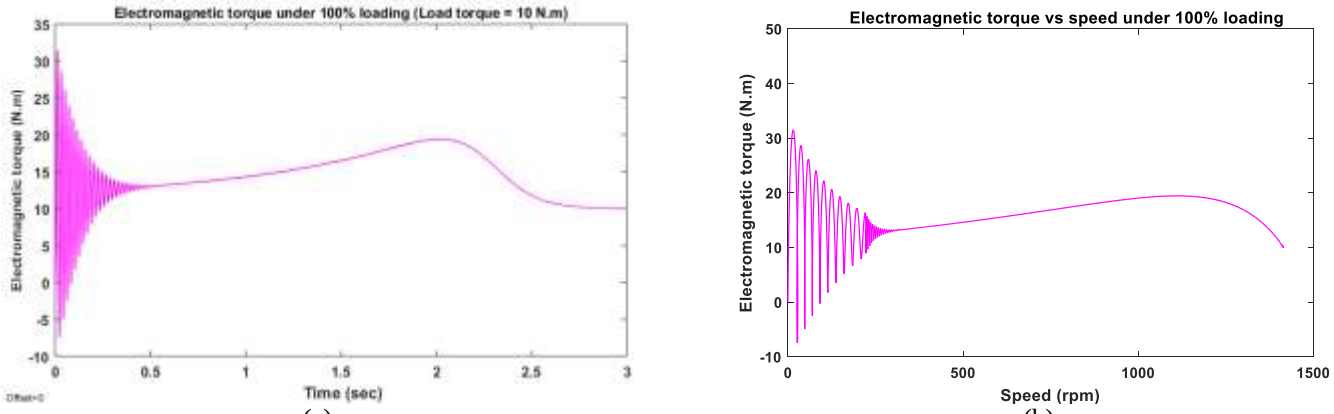

(a) (b)

Fig. 12 *(a) Torque and (b) Torque against speed under 100% loading*

The single cage motor torque plot against time is shown in Fig. 12a under 100% loading condition. The torque curve shows that the motor has a starting of 31.38 Nm but after 2.98 s, a torque of 10 Nm corresponding to the load torque was reached as it began to run at a steady speed.

Figure 12b is the curve of electromagnetic torque against rotor speed for single cage mode simulated in 3 s when the

machine is running under 100% loading. The simulation curve shows that the torque was high during the starting of the motor but decreases as the motor reaches its steady speed less than the rated speed due to loading effect.

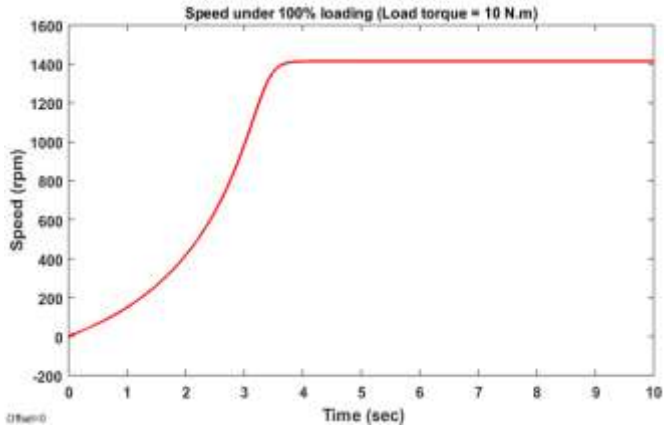

Fig. 13 Motor Speed under 100% loading

Figure 13 single cage rotor speed transient characteristic of during 100% loading. The speed response curve indicates that due to full loading, the speed of the motor dropped from the rated value (1500 rpm) to 1415 rpm. Thus, the effect of the full loading on the speed of the motor is 5.7% drop in rated speed.

With full load scenario considered (that is 100% load torque), it takes 1.4 s longer for the single cage motor to reach steady-state than with 50% load torque as shown in Figures 11 and 12. Figure 13 revealed that the speed of the single cage machine takes approximately 3.5 seconds to reach steady-state. Generally, the rise time in this case was 2.18 s and the settling time was 2.98 s.

5. CONCLUSION

In this work, the d-q reference axis technique was utilized to implement both the static and dynamic performance of a three-phase squirrel cage induction machine of 3.73 kW rated capacity, operating speed of 1500 rpm, phase to phase voltage of 400 V, and with operating frequency of 50 Hz. The machine was configured for single cage operation. The steady-state transient characteristic of the machine as a single cage motor were presented in terms of stator current, rotor current, electromagnetic torque, electromagnetic torque versus speed, and speed for no load, 50% loading (half load), and 10% loading (full-load) scenarios. The simulation analysis indicated that the transient characteristics of the machine drops as the load torque increases.

REFERENCES

[1] Veltman (2006). Interaction between A. C. machine and switching power converters. PhD thesis, Technical University Del.

[2] Ćalasan, M., Micev, M., Ali, Z. M., Zobaa, A. F., & Abdel Aleem, S. H. E. (2020). Parameter estimation of induction machine single-cage and double-cage models using a hybrid simulated annealing–evaporation rate water cycle algorithm. *Mathematics, 8,* Article ID 1024,1-29.

[3] Chitra, V. & Prabhakar, R. (2006). Induction motor speed control using fuzzy logic controller. *World Academy of Science, Engineering and Technology, 23,* 17–22.

[4] Elnaghi, B. E., Mohammed, R. H., Dessouky, S. S., & Shehata, M.K. (2019). Load test of induction motors based on PWM technique using genetic algorithm. *International Journal of Engineering and Manufacturing, 9*(1), 24-32.

[5] Gübahçe, M. O. & Karaasian, M. E. (2022). Estimation of induction motor equivalent circuit parameters from manufacturer's datasheet by particle swarm optimization algorithm for variable frequency drives. *Electrica, 22*(1), 16-26.

[6] Jirdehi, M. A., & Rezaei, A. (2016). Parameters estimation of squirrel-cage induction motors using ANN and ANFIS. *Alexandria Engineering Journal, 55,* 357–368.

[7] Diao, T. (2015). Study on dual-rotor permanent magnet induction motor andperformance. *The Open Electrical & Electronic Engineering Journal, 9,* 954-590.

[8] Salkumar, V. V., Sathyavani, B., & Suresh, J. (2020). Mathematical modeling of five-phase and three-phase induction motor and their result comparison. *IOP Conf. Series: Materials Science and Engineering,* 981 (2020) 042059.

[9] Ogunjuyigbe, A. S. O., Ayodele, T. R., &Adetokun, B. B. (2018). Modelling and analysis of dual stator-winding induction machine usingcomplex vector approach. *Engineering Science and Technology, an International Journal, 21,* 351–363

[10] Hong, C. & Hwang, G. (2012). Transient and steady state performance of squirrel cage induction machine.

[11] Le Roux, P. F. & Ngwenyama, M. K. (2022). Static and dynamic simulation of an induction motor using Matlab/Simulink. *Energies,* 15, 3564, 1-21.

[12] Idoko, A. A., Thuku, I. T., Musa, S. Y., & Amos, C. (2017). Design of tuning mechanism of PID controller for application in three phase induction motor speed control. *International Journal of Advanced Engineering Research and Science, 4*(11), 138 – 146.

[13] Malatji, M. M. (n. d.). Derivation and implementation of a DQ model of an induction machine using MATLAB/Simulink. *Electromechanical Conversion,* Technical Report, 1-8.

[14] Leedy, A. W. (2013). Simulink/MATLAB dynamic induction motor model for use in undergraduate electric machines and power electronics courses, 2013 Proceedings ofIEEE Southeastcon, Jacksonville, FL, 1-6.